HOSTED BY
ELSEVIER
Available online at www.sciencedirect.com
ScienceDirect
Soils and Foundations 59 (2019) 380–397
www.elsevier.com/locate/sandf

Empirical fragility curves for settlement-affected buildings: Analysis of different intensity parameters for seven hundred masonry buildings in The Netherlands

Dario Peduto [a], Mandy Korff [b,c], Gianfranco Nicodemo [a], Antonio Marchese [a], Settimio Ferlisi [a,*]

[a] Department of Civil Engineering, University of Salerno, via Giovanni Paolo II, 132, 84084 Fisciano (SA), Italy
[b] Deltares, P.O BOX, 177, 2600 MH Delft, The Netherlands
[c] Delft University of Technology, Faculty of Civil Engineering and Geosciences, Stevinweg 1, 2628 CN Delft/2600 GA Delft, The Netherlands

Received 17 April 2018; received in revised form 29 October 2018; accepted 3 December 2018
Available online 6 March 2019

Abstract

The analysis and prediction of damage to buildings resting on highly compressible fine-grained "soft soils" containing (organic) clay and peat are key issues to be addressed for a proper management of subsidence-affected urban areas. Among the probabilistic approaches suggested in literature, those oriented to the generation of empirical fragility curves are particularly promising provided that a comprehensive dataset for both the subsidence-related intensity (SRI) parameters and the corresponding damage severity to buildings is available. Following this line of thought, in the present paper, a rich sample of more than seven hundred monitored (by remote sensing) and surveyed masonry buildings – mainly resting with their (shallow or piled) foundations on soft soils – is analysed in four urban areas of The Netherlands. Probabilistic functions in the form of fragility curves for building damage are retrieved for three different SRI parameters (i.e., differential settlement, rotation and deflection ratio) derived from the processing of Synthetic Aperture Radar (SAR) images by way of a differential interferometric (DInSAR) technique in combination with the severity levels of the damage recorded from the visual inspection of over 700 masonry buildings. As a novelty with respect to earlier similar studies, the work points out the methodological steps to be followed in order to identify the most appropriate SRI parameter among the selected ones. Thus, the objective of the paper is to improve the existing geotechnical forecasting tools for subsidence-affected urban areas, in order to target areas that require more detailed investigations/analyses and/or to select/prioritize foundation repairing/replacing measures.

Keywords: Soft soils; Settlements; Shallow/piled foundations; Fragility curves; DInSAR

1. Introduction

Ground settlements related to the subsidence phenomena of either natural or anthropogenic origin, or complex combinations of both, cause damage to affected facilities (e.g., buildings) resulting in economic losses of billions of US Dollars per year (Holzer, 2009; Bucx et al., 2015). For this reason, scientists, technicians, politicians and civilian communities are interested in studies aimed at analysing and predicting the consequences of damage to

Peer review under responsibility of The Japanese Geotechnical Society.
* Corresponding author.
E-mail addresses: dpeduto@unisa.it (D. Peduto), mandy.korff@deltares.nl, M.Korff@tudelft.nl (M. Korff), gnicodemo@unisa.it (G. Nicodemo), amarchese@unisa.it (A. Marchese), sferlisi@unisa.it (S. Ferlisi).

https://doi.org/10.1016/j.sandf.2018.12.009
0038-0806/

buildings in subsiding areas in order to select the most suitable strategies for land-use planning and urban management purposes. The availability of information on the spatial distribution and severity of damage suffered by buildings, as well as their displacement rates, is crucial to the above studies. In addition to conventional monitoring techniques, like topographic levelling, tachymetry and global navigation satellite systems (GNSS), useful information on displacement rates can be derived from processing images acquired by spaceborne Synthetic Aperture Radar (SAR) sensors via advanced differential interferometric techniques (generically called "DInSAR"). DInSAR-derived displacement rates are currently available over a large number of buildings, and recent works by the authors (Peduto et al., 2016a, 2017c, 2018b) show that they can be successfully combined with the results of damage surveys to generate empirical fragility curves. The latter, as a rule, provide the conditional probability of reaching or exceeding a certain damage severity level as a function of a subsidence-related intensity (SRI) parameter that affects a generic (i.e., randomly selected) building – belonging to a homogeneous set of surveyed buildings – over a given period of time.

The key idea of the present work is to evaluate the use of different SRI parameters – whereas previous works focused on one parameter only (Peduto et al., 2016a, 2017c) – by carrying out a feasibility test aimed at identifying the SRI parameter (amongst three) that best fits the damage analysis and prediction for large quantities of houses. In particular, the procedure introduced by Peduto et al. (2017c) was improved to derive (from DInSAR data) the investigated SRI parameter – i.e., differential settlement, rotation and deflection ratio (Burland and Wroth, 1974) – to be combined with a rich dataset of information gathered from in-situ damage surveys conducted on more than seven hundred masonry buildings with both shallow and piled foundations in four cities in subsiding areas of The Netherlands.

The selected cities are situated in areas that suffer from widespread ground settlements (Papadaki, 2013) mainly associated with the presence of highly compressible fine-grained "soft soils", e.g., clay and peat in the upper strata (Den Haan and Kruse, 2006). The subsidence-related problems are often exacerbated by decay processes (due to fungal or bacteria attack) affecting wooden piles (Klaassen and Creemers, 2012). Foundations in the study areas consist of both shallow and piled systems, whose functionality under live loads can be so seriously compromised that, with the passing of time, costly measures to maintain/repair/replace them have to be undertaken in order to prevent the serviceability/ultimate limit states of the buildings.

2. Damage assessment and classification

Empirical relationships between the displacements of foundations and the damage induced to superstructures have been developed by several researchers. Early on, Skempton and MacDonald (1956) reported observations of settlements and the onsets of cracking to 98 buildings with isolated/continuous footings resting on fine-/coarse-grained soils, while Polshin and Tokar (1957) suggested a damage criterion based on 25 years of Soviet experience. Bjerrum (1963) first retrieved useful relationships between the maximum settlement and the maximum differential settlement, and recommended the limiting values of angular distortions for buildings. Grant et al. (1974) enlarged the settlement and damage database (available at that time) with an additional sample of 95 buildings. Burland and Wroth (1974) addressed the conditions leading to settlement-induced damage and, similar to Polshin and Tokar (1957), concluded that visible cracking is related to the exceedance of certain values of tensile strain.

Based on the above-mentioned damage criteria, placing a limitation on the values of some SRI parameters (e.g., angular distortion/relative rotation) is currently used in several design codes (AASHTO, 1997; CEN, 2004).

The state of the art on building damage for masonry buildings is mainly based on the work of Boscardin and Cording (1989) and Burland (1995); it is more commonly known as the Limiting Tensile Strain Method (LTSM). This method is generally adopted in the cases of tunnelling or other ground-related works. The LTSM involves classifying the damage severity according to the system proposed by Burland et al. (1977) for brickwork or blockwork and stone masonry, which mainly reflects the attainment of damage affecting the building aesthetics (D0 = negligible, D1 = very slight and D2 = slight), causing a loss of functionality (D3 = moderate and D4 = severe) or even compromising the stability (D5 = very severe). According to LTSM, a given damage severity level is attained if the combination of bending, shear and horizontal strain (combined into one tensile strain) reaches a certain limiting value. Factors influencing the limiting values of the tensile strain are, for example, the geometrical and mechanical characteristics of the building (Son and Cording, 2007).

The main question that this paper aims to address is whether or not these approaches also work for large numbers of buildings for which limited information is available. Considering the inherent uncertainties involved in the problem, an interesting perspective is offered by probabilistic tools relating different (measured) SRI parameter values with (surveyed) damage severity levels in the form of empirical fragility curves. For the latter, following an approach adopted in the earthquake engineering field (Gehl et al., 2015; Shinozuka et al., 2000), a lognormal distribution is usually assumed (Ferlisi et al., 2018; Peduto et al., 2016a, 2016b, 2017a, 2017c; Saeidi et al., 2012):

$$P(Damage \geq Di|SRI) = \Phi\left[\frac{1}{\beta_i}\ln\left(\frac{SRI}{\overline{SRI}_i}\right)\right] \quad (1)$$

where $P(\cdot)$ is the probability of reaching/exceeding a certain damage severity level Di for a given value of SRI, Φ [ ] is the standard normal cumulative distribution function, and $\overline{SRI}_i$ and β_i, respectively, represent the median and the

standard deviation (or fragility parameters according to Shinozuka et al., 2003) of the lognormal distribution for each damage severity level, Di.

3. DInSAR data and accuracy test

Spaceborne Synthetic Aperture Radar (SAR) images, processed via advanced differential interferometric techniques (DInSAR), are currently widely used to detect and analyse ground displacements associated with either natural or anthropogenic phenomena. Some recent pioneering examples of its application in geotechnical modelling have combined subsoil and settlement modelling with the information gathered by DInSAR-derived ground displacements (Castaldo et al., 2015; Modoni et al., 2013; Peduto et al., 2017b). In this work, Persistent Scatterer Interferometry (PSI) techniques (Costantini et al., 2008; Ferretti et al., 2001) are used to identify reliable scatterers (e.g., buildings). In particular, PSI-retrieved displacements are provided, with reference to a ground point, along the radar line of sight (LOS) with sub-millimetre precision (Hanssen, 2003) or accuracy (Nicodemo et al., 2016; Peduto et al., 2017b, 2018a) on the average velocity and sub-centimetre accuracy of the single displacement measurement (Herrera et al., 2009). For the specific purpose of ground displacement monitoring in built-up urban areas, X-band high-resolution SAR sensor TerraSAR-X (TSX) and COSMO-SkyMed recently proved to be suitable for the precise monitoring of single structures/infrastructure (Cascini et al., 2013; Fornaro et al., 2013, 2014; Nicodemo et al., 2016; Peduto et al., 2015, 2017b, 2017c, 2018a; Reale et al., 2011; Zhu and Bamler, 2010).

In the present study, the availability of a large quantity of both DInSAR and topographic levelling data on the Schiedam-West neighbourhood in the city of Schiedam (The Netherlands) allowed for the performance of an accuracy test of the used dataset. The latter consists of 285 images (133 on the ascending orbit and 162 on the descending orbit) acquired via the stripmap mode by the TerraSAR-X constellation of satellites spanning the period 2009–2014 (Peduto et al., 2017c). Moreover, long-term measurements from four hundred levelling benchmarks on building façades are available. These data, covering ten years starting from 2004, were filtered in the same period as the DInSAR data (2009–2014) and only the levelling time series with a minimum frequency of one measurement per year is considered for the comparison. Then, permanent scatterers (PSs) within a 2-m spatial buffer around a single levelling point are selected in order to take into account the localization error of the DInSAR measurements. Adopting these criteria, 83 levelling benchmarks are used in the analysis and their velocity values over the observation period are compared with the average velocity value of all the selected PSs (on both ascending and descending orbits) falling within the 2-m spatial buffer around the levelling point (Fig. 1a). The accuracy of the DInSAR velocity for the test area is computed in terms of the difference between the DInSAR and the levelling data (ΔV) for each considered benchmark. A histogram of the DInSAR accuracy is shown in Fig. 1b, with an average value equal to 0.85 mm/year and a standard deviation of 0.55 mm/year. Accordingly, the 1-sigma accuracy can be set to 1.40 mm/year, thus confirming for the case study at hand the results from other authors (e.g., Herrera et al., 2009; Peduto et al., 2018a).

For the sake of completeness, the relationship between the quality parameter of the PS dataset and the ΔV values is also investigated. The PS quality parameter is representative of the conformity (namely, coherence) between the measured DInSAR data and the displacement model used in the DInSAR analysis phase. It can fall in the range of 0 (points lacking conformity with the model and which are therefore unreliable) to 1 (points with high conformity with the model and which are therefore reliable). A low coherence value does not necessarily indicate a high noise level of the data, but can be caused by types of motion that deviate from the linear motion model. As shown by the diagrams in Fig. 1c, it is possible to derive which average value ΔV and related standard deviation are expected for a given range in the quality parameter. Indeed, the ΔV value decreases as the quality parameter increases; therefore, the higher the quality parameter is the more accurate the DInSAR data are. This means that DInSAR data are considered accurate enough to derive the fragility curves for the different building and foundation types.

4. Methodology

The procedure followed for the analyses consists of three phases preceded by a preliminary data preparation phase (Fig. 2). In particular, the PSI data are divided into the PSs on top of buildings and the PSs at ground level, and the accuracy test described in Section 3 is conducted in order to check whether the limiting value proposed in literature (i.e., 1.5 mm/year) is satisfied. Then, if the PSs on top of buildings fall within a 2-meter buffer around the building's perimeter, it is deemed that they are associated with that building (Fig. 3a). In Phase I-A, the cumulative settlement pertaining to each PS over the observation period is derived by multiplying the available PS velocity by the monitoring period. In this way, settlements are implicitly assumed as occurring at a constant rate in the study area during the observation period. This assumption is acceptable if such widespread settlements in the analysed areas are considered to be mainly related to the long-term creep processes (Den Haan and Kruse, 2006; Peduto et al., 2017c). PS-derived settlement data are interpolated over each building on a grid, 2 m × 2 m, so that settlement profiles can be retrieved along selected sections, i.e., parallel to the road in the case study at hand, as shown in Fig. 3a.

Once the settlement profile is derived, different SRI parameters for the foundation movement are computed. It is worth stressing that settlements refer to the PSs located on the roof of the building. Hereafter in the study, how-

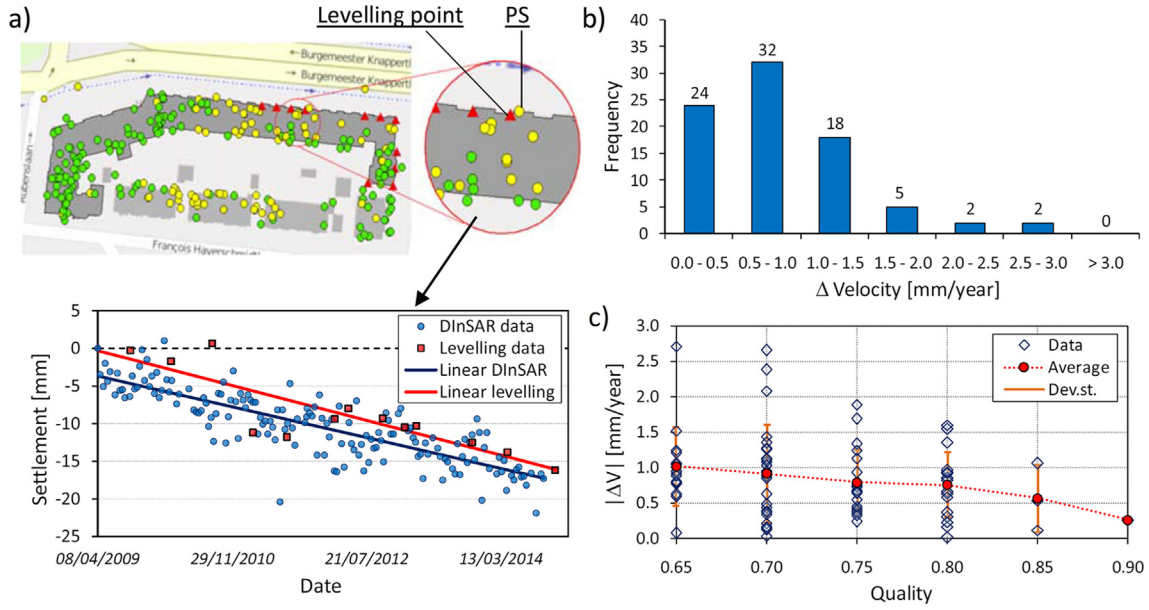

Fig. 1. DInSAR data accuracy test: (a) comparison of the time series derived for a levelling benchmark and a PS within a 2-m buffer around the levelling point in the period 2009–2014; (b) ΔV frequency distribution of the difference between DInSAR and the levelling velocities; (c) PS quality vs. ΔV recorded in the observation period.

ever, they are considered as occurring at the foundation level, thus disregarding either compressive or tensile strain that may affect the superstructure (Cascini et al., 2007). Accordingly:

- differential settlement δρ is computed along the profile as the difference between the maximum and the minimum values of the recorded settlements (Fig. 3b);
- the rotation (θ), or slope, is assumed as $\theta = \delta\rho/L_\rho$, where L_ρ indicates the distance at the foundation level between the two points where δρ was computed (Fig. 3b);
- the deflection ratio is obtained as Δ/L according to the definitions provided by Burland and Wroth (1974), where Δ is the displacement of a point relative to the line connecting two reference points and L is the distance between these two points.

For the evaluation of the deflection ratio, the locations of the reference points are critical. Since defining the positions of these points is not straightforward from the DInSAR data, two different values for the deflection ratio (Δ_1/L_1 and Δ_2/L_2) are defined in the present analysis (Fig. 3c and d), as follows:

1. In the simplified approach, the deflection ratio is given by Δ_1/L_1, Δ_1 being the displacement of a point relative to the line connecting two consecutive points of intersection between the line (that joins the two extremities of the building foundation with a distance L) and the settlement profile, and L_1 being the distance between two consecutive points of intersection. In particular, as shown in Fig. 3c, the values for $(\Delta_{1s}/L_{1s})_{max}$ and $(\Delta_{1h}/L_{1h})_{max}$, in the sagging and hogging zones, respectively, are estimated for every building, and the largest values for these two $[(\Delta_1/L_1)_{max} = \max\{(\Delta_{1s}/L_{1s})_{max}; (\Delta_{1h}/L_{1h})_{max}\}]$ are associated with the corresponding damage severity level of a given building, taking into account that a single damage severity level was identified for a single building.
2. The standard/original approach for the deflection ratio – according to the definition provided by Burland and Wroth (1974) – is obtained as Δ_2/L_2 with Δ_2 being the displacement of a point relative to the line connecting two consecutive inflection points, and L_2 being the distance between two consecutive points of inflection (see also Burland et al., 2004; Franzius et al., 2004). In Fig. 3d, the values for $(\Delta_{2s}/L_{2s})_{max}$ and $(\Delta_{2h}/L_{2h})_{max}$, in the sagging and hogging zones, respectively, are estimated for every building, and the largest values for these two $[(\Delta_2/L_2)_{max} = \max\{(\Delta_{2s}/L_{2s})_{max}; (\Delta_{2h}/L_{2h})_{max}\}]$ are associated with the corresponding damage severity level of a given building.

A further essential step is the use of visually obtained damage surveys (Phase I-B). For this purpose, fact sheets, to be completed during the in-situ surveys (Peduto et al., 2017c), allow for the collection of information about the location of a certain building and its description in terms of structural type, foundation typology (i.e., shallow or piled), number of floors, age of construction and occupancy type, the available datasets on the geological features and PSI data, photos of the damage experienced by the building façades (in terms of cracks and/or disjunction in

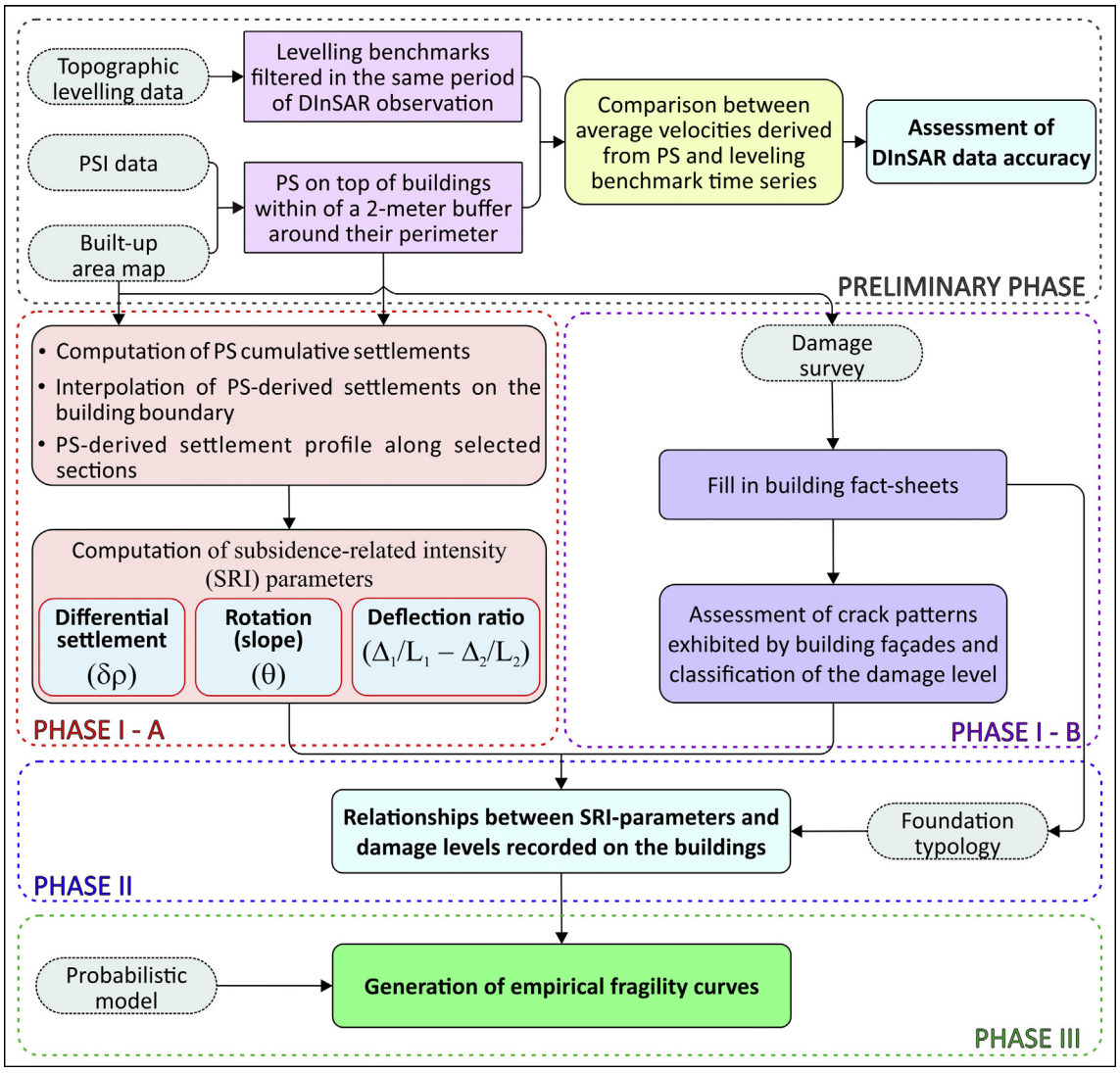

Fig. 2. Flowchart of the methodology.

the outer walls and their position, distortions or tilt) and, finally, the damage severity level assigned on the basis of the classification system provided by Burland et al. (1977).

In Phase II, the empirical relationships between the magnitude of the selected SRI parameters and the level of damage severity assigned during the surveys are developed for all the analysed (706) masonry buildings with shallow or piled foundations.

In Phase III, using Eq. (1), the empirical fragility curves are generated and evaluated for different SRI parameters pertaining to masonry buildings resting on either shallow or piled foundations.

The fragility parameters (i.e., $\overline{SRI}_i$ and β) are computed following the procedure proposed by Shinozuka et al. (2003). In particular, a unique β value is adopted in order to have coherent probabilities for the different damage levels (Fotopoulou and Pitilakis, 2013). The maximum likelihood (ML) method is used to estimate the fragility parameters as those that maximize the likelihood of fitting with "real" data. As β is taken to be equal for all damage levels, the likelihood function can be expressed as follows (Mavrouli et al., 2014; Shinozuka et al., 2003):

$$L\left(\overline{SRI}_i, \beta\right) = \prod_{j=1}^{N} \prod_{i=0}^{k} P_i\left(SRI_j; D_i\right)^{y_{ji}} \quad (2)$$

where $P_i = P(SRI_j, D_i)$ is the probability that the j-th (randomly selected) building from the sample will be at damage level D_i when subjected to the SRI_j parameter value. D_i, in turn, indicates the considered damage severity level with i falling in the range of 0 to k ($k = 0, 1, 2, 3$ for the sample of buildings resting on shallow foundations and $k = 0, 1, 2, 3, 4$ for buildings resting on piled foundations); $y_{ji} = 1$ if damage level D_i occurs for the j-th building subjected to intensity value SRI_j; otherwise $y_{ji} = 0$.

Finally, the fragility parameters are obtained by solving the following equations to maximize the likelihood function (Shinozuka et al., 2003):

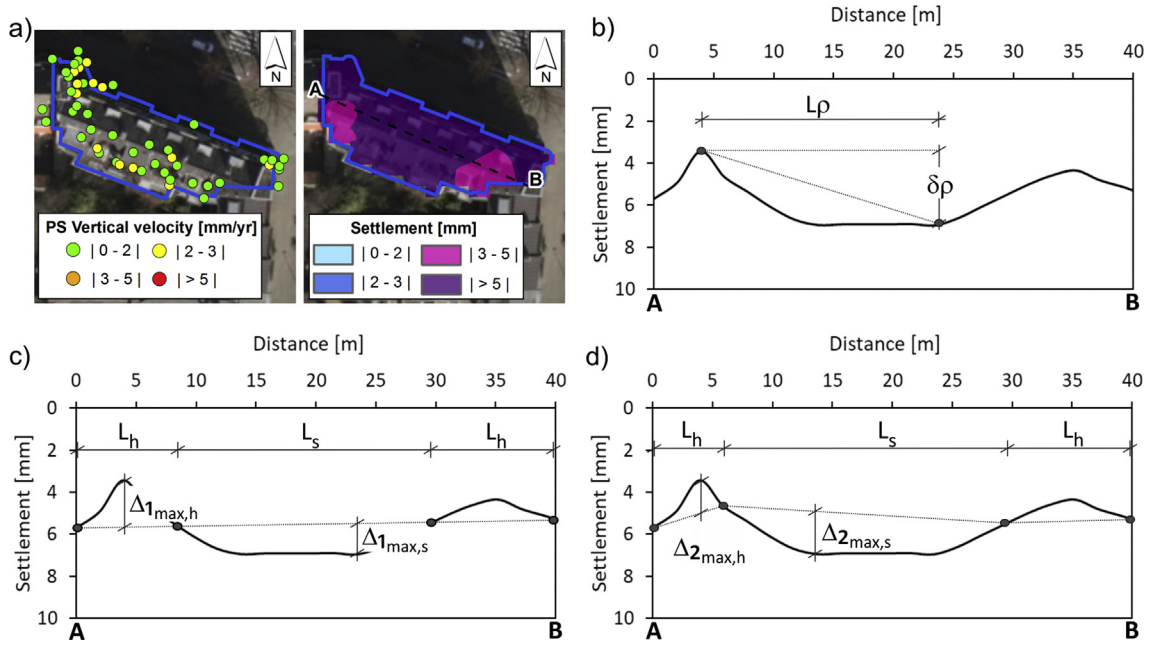

Fig. 3. Sketch synthesizing the computation of the DInSAR-derived SRI parameters: (a) map of PS vertical velocities and cumulative settlements; (b) differential settlements δρ and Lρ; (c) deflection ratio as Δ_1/L_1; (d) deflection ratio as Δ_2/L_2.

$$\frac{\partial lnL\left(\overline{SRI}_i,\beta\right)}{\partial \overline{SRI}_i}=\frac{\partial lnL\left(\overline{SRI}_i,\beta\right)}{\partial \beta}=0 \tag{3}$$

5. Case study areas

The Netherlands, a low-lying river delta close to the North Sea, has a number of distinct geographic regions determined by their dominant soil profile (Hartemink and Sonneveld, 2013). About half of the country's surface is found below sea level (''Normal Amsterdam Level", N.A.P.). The four main rivers (Rhine, Meuse, Scheldt and IJssel) and the sea have shaped the Dutch Holocene depositionary environment. As a result, the subsoil consists of highly compressible soils in the western and northern regions (Fig. 4), and Pleistocene deposits – mainly made up of sandy soils sloping upwards to the south (van der Meulen et al., 2013) – prevail in the east. In the last few decades, the Geological Survey of The Netherlands (GDN) has systematically collected and analysed hundreds of thousands of borehole data and cone penetration tests (Stafleu et al., 2011) that allowed the generation of the nationwide 3D geological 'GeoTOP' model (DINOloket, 2016). In particular, this model schematizes the Dutch subsoil into millions of voxels (100 × 100 × 0.5 m, height × width × depth) providing information on the litho-stratigraphy (including the probability of the occurrence of each lithological class) down to a depth of 50 m below the ground surface.

In the present study, 706 masonry buildings with shallow and (mainly wooden) piled foundations, belonging to four municipalities, are analysed (Fig. 4). The municipalities are Zaanstad, Rotterdam, Schiedam and Dordrecht. They are all located within areas where large deposits of soft soils are present. The analysed building stock consists of low-rise masonry buildings (2–3 floors), the ages of which date back to the beginning of the 19th century up to about the 1980s, mainly constructed out of brick and lime mortar.

As for the DInSAR data used in the analyses, they were provided by SkyGeo Netherlands B.V. that developed a commercial chain 'Antares' – mainly based on the PSI method (Ferretti et al., 2001) – for processing SAR images, in this case acquired by the TerraSAR-X satellite constellation via the stripmap mode. As an input Digital Elevation Model (DEM), the SRTM90 (USGS, 2016) was used. Considering the flatness of Dutch topography, the DEM resolution is sufficient for unambiguous height estimations (Bamler and Hartl, 1998) and the subsequent estimations of atmospheric disturbances (Ferretti et al., 2001). Since subsidence-related displacements are assumed to be mainly vertical, the PSI data were projected from the LOS to the vertical direction (Cascini et al., 2007).

5.1. Zaanstad

Zaanstad is a densely urbanized municipality located north of Amsterdam. A generic cross-section along the A-A′ profile (Fig. 5a) shows that the upper part of the subsoil in the Zaanstad area consists of mainly clay and peat, with a cumulative thickness not exceeding 10 m, resting on a sandy deposit that includes some thin lenses of clayey soil or sandy clay (Peduto et al., 2016a). Consequently, in the historic centre of Zaanstad, the masonry buildings mainly rest on wooden piles in order to prevent the loading of the upper highly compressible layers. This town, like most

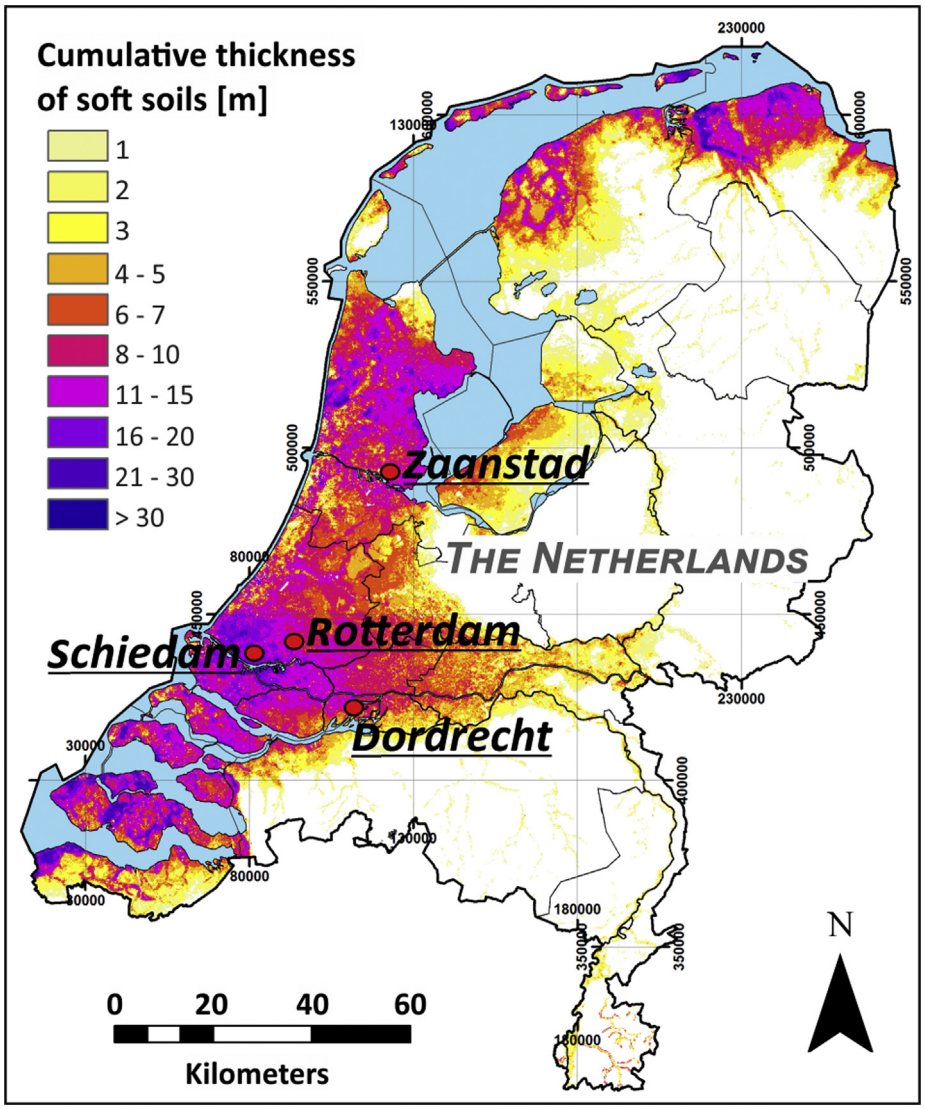

Fig. 4. Locations of the case study areas plotted on the map of the cumulative thickness of soft soils in The Netherlands (courtesy of Deltares).

western cities in The Netherlands, suffers from widespread building foundation problems that prompted the municipality to arrange extensive campaigns for foundation inspections aimed at investigating their conservation state. The results of the inspections highlighted that several piled foundations suffered from the effects of wood decay; and thus, restoration works were promoted.

The available SAR image dataset over Zaanstad consists of 162 TSX images acquired via the stripmap mode on the ascending orbit between 05 February 2009 and 14 October 2015.

Fig. 5b shows the PSI data over the two selected parts of Zaanstad that exhibited the highest settlement rates in the period of observation. Fig. 5c shows a map of the buildings that were surveyed between February and March 2016. All eighty-one of the surveyed buildings rest on piles. Fig. 5e and f show some photos of the buildings; Fig. 5d displays the distribution of damage levels. The number of buildings per damage severity level is: D0 = 8, D1 = 31, D2 = 20, D3 = 16, D4 = 6 and D5 = 0.

5.2. Rotterdam

The city of Rotterdam is located in the southwestern part of The Netherlands (Fig. 6a), in an area that is a section of the Rhine-Meuse Delta system. The upper 20 m of the subsurface consist of unconsolidated, Holocene sediments, deposited in fluvial and coastal environments. As shown in Fig. 6a, there are alternating layers of organic material and clay (i.e., soft soils) from the ground level to a depth that varies between 5 and 16 m. Subsidence is a widespread problem in the Rotterdam area, leading to high societal costs, such as those related to adaptation measures in water management and repair costs for damaged buildings and the infrastructure. There is ample evidence of this damage, including the flooding of cellars, parks and roads, as well as the settlement of buildings.

For the area of Rotterdam, the available SAR dataset consists of 285 images acquired via the stripmap mode by the TerraSAR-X constellation of satellites spanning the period of 2009–2014. The images are from two separate

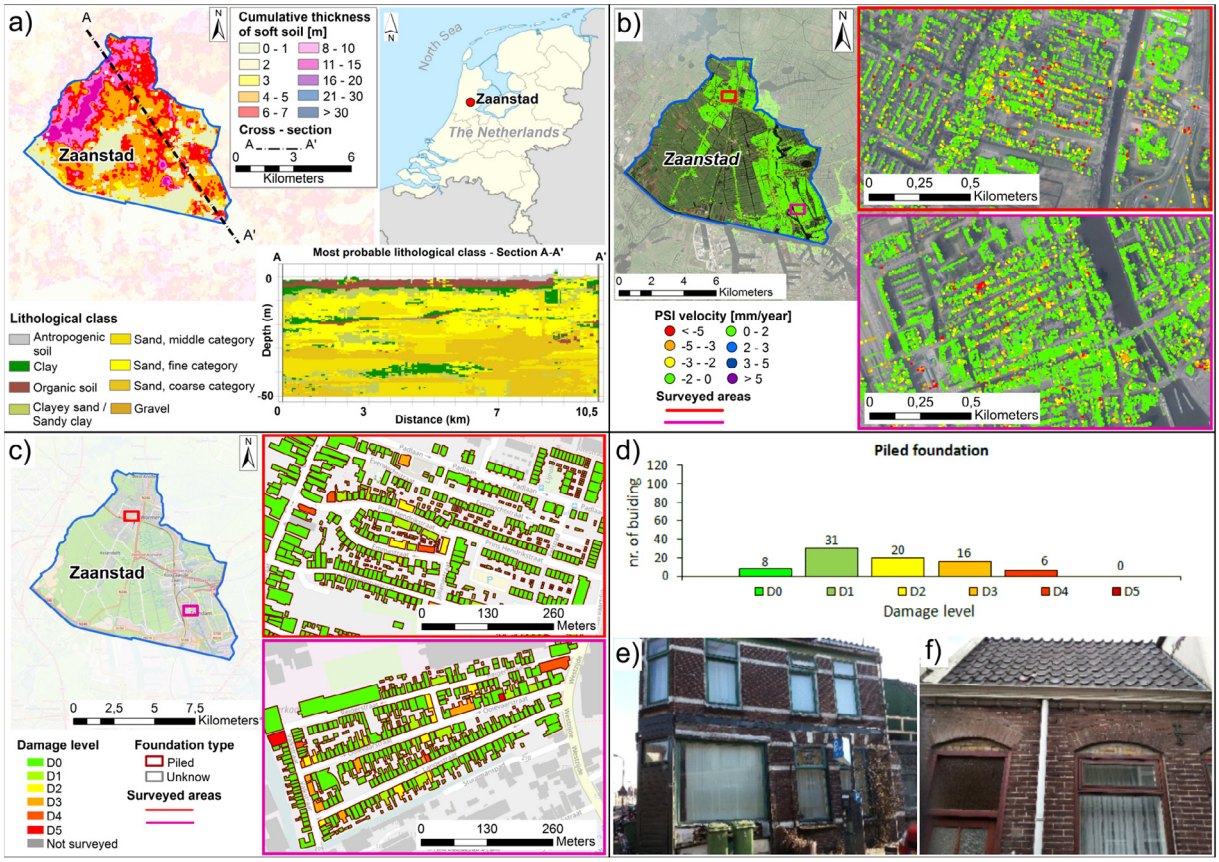

Fig. 5. Zaanstad case study: (a) cumulative thickness of soft soils (organic and clayey) and geological cross-section along the A–A' profile sketch; (b) PSI data on the ascending orbit on top of the buildings provided by the TSX radar sensor; (c) map of the surveyed masonry buildings distinguished according to the assigned damage severity level, foundation type and their distribution for (d) piled foundations; (e) and (f) some photos of cracks and deformation revealed on building façades during the in-situ surveys.

datasets: 133 from the ascending orbit and 162 from the descending orbit (Peduto et al., 2017c). In particular, analyses focusing on two different areas of Rotterdam (Fig. 6b and c), where 183 buildings are located (125 belong to the first study area and 58 to the second one), were conducted. As shown on the PSI velocity map in Fig. 6b, the PSs located on the top of the buildings in these areas measured deformation rates higher than 5 mm/year.

As a result of an extensive visual damage inspection carried out from June to July 2016 (Fig. 6c–f), 183 masonry buildings for which PSI data are available, all resting on (mainly wooden) piled foundations, were each assigned a damage severity level (Fig. 6c) whose distribution is shown in Fig. 6d. Out of the 183 buildings, 81 buildings exhibited some level of damage. The number of buildings per damage severity level is: D0 = 102, D1 = 43, D2 = 18, D3 = 11, D4 = 9 and D5 = 0.

5.3. Schiedam

The study area is a 2-km^2 densely urbanized neighbourhood in the southwestern part of the city of Schiedam, just north of Rotterdam (Fig. 7). The subsoil is composed of a stratified deposit of the Holocene age, including layers of clay and peat whose cumulative thickness does not exceed 20 m, laying on a sandy layer (Fig. 7a). Below this sandy layer, soft cohesive soils are mixed with narrow lenses of sandy soil resting on a sand deposit of the Pleistocene age. A sample cross-section of the subsoil in the area, as derived from the GeoTOP model, is shown in Fig. 7a.

For the area of Schiedam, the same TSX images as those over the Rotterdam area were used. A map of the PSI data with the measured deformation velocities is shown in Fig. 7b.

As for the damage to buildings, in-situ surveys were carried out in April and May of 2015. These surveys focused on 310 single buildings (most of them being part of row-houses) (Fig. 7c) built in masonry – typical of the local architecture – resting on either shallow or piled foundations. Fig. 7c shows a map of the surveyed buildings distinguished according to their foundation typology (104 shallow and 206 piled) together with the distribution of the assigned damage severity levels (Fig. 7d and e) and some photos of cracks in building façades and sidewalks taken during the in-situ surveys (Fig. 7f and g). The survey of buildings with shallow foundations revealed the existence of 51 buildings with damage. The number of buildings per damage severity level is: D0 = 53, D1 = 21, D2 = 24, D3 = 6, D4 = 0 and D5 = 0. Out of the 206 surveyed buildings with piled foundations, 94 buildings with

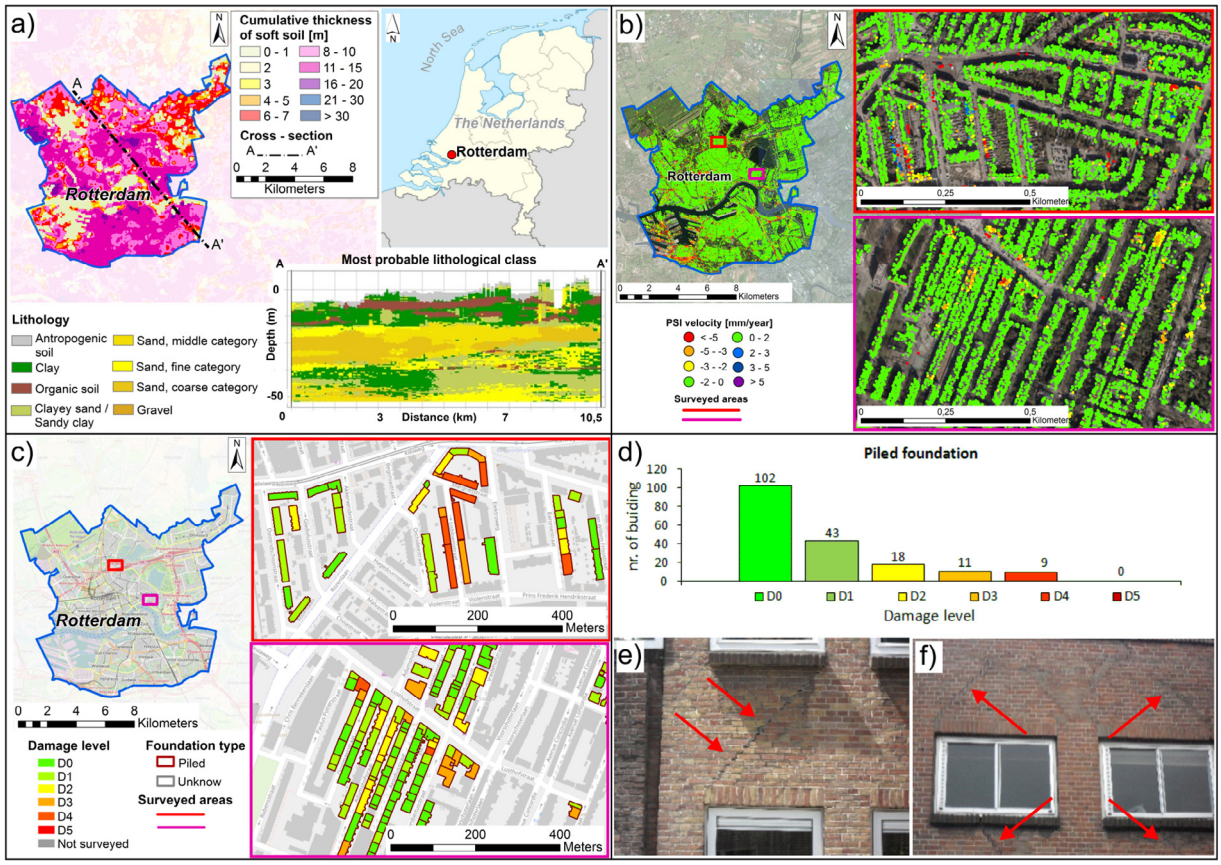

Fig. 6. Rotterdam case study: (a) cumulative thickness of soft soils (organic and clayey) and geological cross-section along the A–A' profile sketch; (b) PSI data on the ascending and descending orbits on top of the buildings provided by the TSX radar sensor; (c) map of the surveyed masonry buildings distinguished according to the assigned damage severity level, foundation type and their distribution for d) piled foundations; (e) and (f) some photos of cracks and deformation revealed on building façades during the in-situ surveys.

damage were identified. The number of buildings per damage severity level is: D0 = 112, D1 = 56, D2 = 33, D3 = 5, D4 = 0 and D5 = 0.

5.4. Dordrecht

Dordrecht is also found in the Rhine-Meuse Delta system, about 20 km southeast of Rotterdam (Fig. 8a). The subsoil consists mainly of alternating soft cohesive and sandy layers, a few metres in thickness each (Fig. 8a). In particular, there are alternating layers of organic material and clay from the ground surface to a depth that varies between 5 and 12 m (Peduto et al., 2016a). Typical for this city is the mix of buildings with shallow foundations and (wooden) piled foundations. Substantial land subsidence has taken place in the past, in part related to groundwater lowering. Owing to the damage suffered by the affected buildings, the municipality of Dordrecht fostered an investigation aimed at inspecting the type of foundations and their state of preservation. The same TSX dataset as that used for Zaanstad allowed for the retrieval of the PSI data shown in Fig. 8b. The sample of surveyed buildings, distinguished according to the assigned damage severity level (Fig. 8c–g), consists of 132 masonry structures, of which 76 have a shallow foundation (the number of buildings per damage severity level is: D0 = 56, D1 = 9, D2 = 5, D3 = 6, D4 = 0 and D5 = 0; see Fig. 8d) and 56 have a piled foundation (the number of buildings per damage severity level is: D0 = 23, D1 = 16, D2 = 9, D3 = 4, D4 = 2 and D5 = 2; see Fig. 8e).

6. Results

6.1. Phases I and II

For each surveyed building, the values pertaining to the selected SRI parameters were estimated once; they were related to the assigned damage severity level (Phases I-A and I-B in Fig. 2). According to Phase II of the methodology described in Section 4, the results of the four areas were combined into one dataset according to similar subsoil settings and properties as well as foundations and structural typology. This allowed for the retrieving of the empirical relationship between the different SRI parameters and the damage severity levels for a total of 706 masonry buildings (Table 1) with either shallow (180 buildings; Fig. 9a, c, e and g) or piled (526 buildings; Fig. 9b, d, f and h) foundations. The values for the arithmetic mean (μ) and standard deviation (σ) together with the coefficient of variation CV (defined as σ/μ) per each SRI parameter and damage level

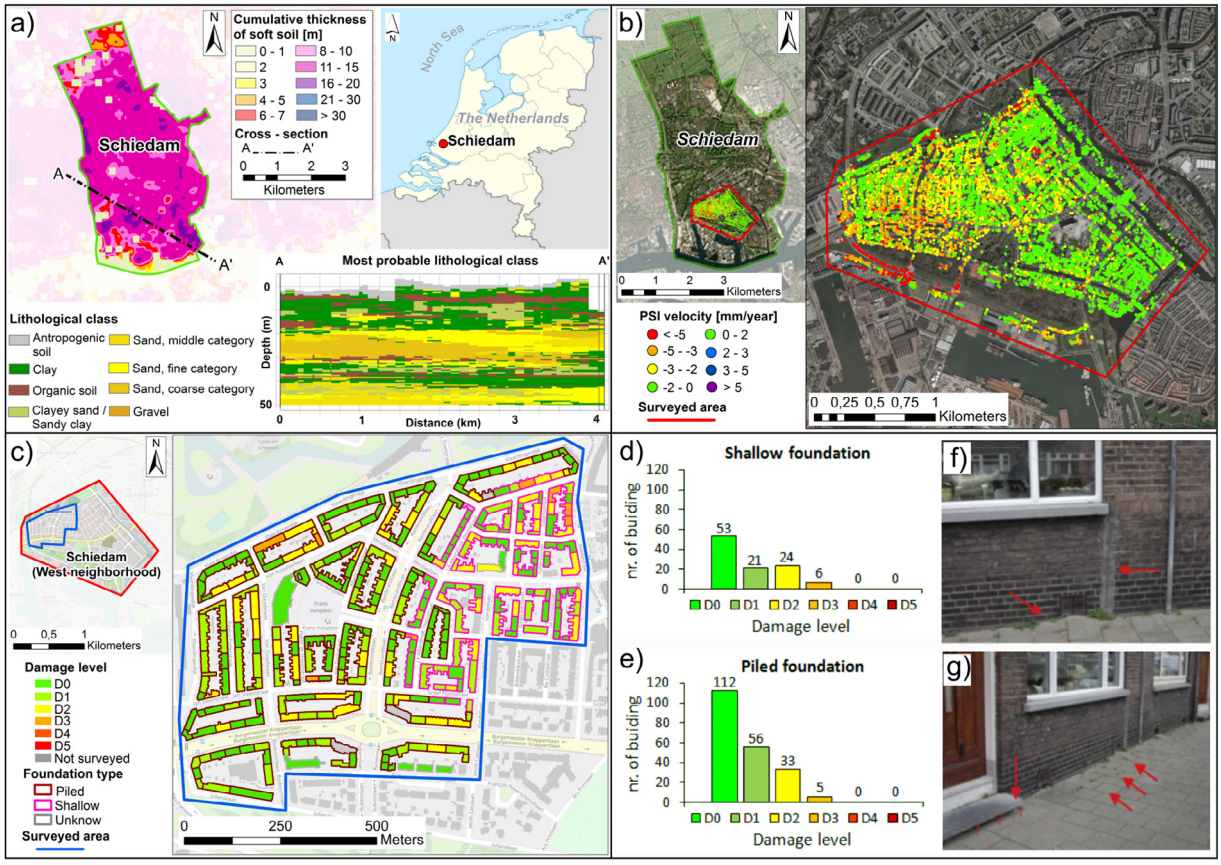

Fig. 7. Schiedam case study: (a) cumulative thickness of soft soils (organic and clayey) and geological cross-section along the A–A' profile sketch; (b) PSI data on the ascending and descending orbits on top of the buildings provided by the TerraSAR-X radar sensor during the period 2009–2014; (c) map of the surveyed masonry buildings distinguished according to the assigned damage severity level, foundation type and their distribution for (d) shallow and (e) wooden pile foundations; some photos of cracks and deformation revealed during the in-situ surveys on (f) building façades and (g) sidewalks.

are provided in Table 2 for both shallow and piled foundations. The data associated with damage severity levels D4 and D5 were merged into a unique damage class (D4-D5) because the number of buildings falling in each of these classes was too small for a reliable probabilistic analysis. In this regard, it is worth observing that the highest damage severity level (D4-D5) was recorded only for buildings resting on piled foundations.

On the whole, the obtained relationships show that the damage severity level generally increased as any of the selected SRI parameters increased.

6.2. Phase III

In Phase III, by using the cumulative log-normal distribution function (Eq. (1)), empirical fragility curves relevant to four SRI parameters were derived for the two foundation types (shallow in Fig. 10b, d, f and h and piled in Fig. 11b, d, f and h). For this purpose, the frequency of the occurrence of each level of damage severity was calculated for the different SRI parameters derived from the DInSAR data (see Fig. 10a, c, e and g for shallow foundations and Fig. 11a, c, e and g for piled foundations). The fragility parameters (i.e., $\overline{SRI}_i$ and β) were computed following the procedure proposed by Shinozuka et al. (2003) using Eqs. (2) and (3). The parameters for the corresponding functions are given in Table 3.

7. Discussion

The analyses presented in the above section allowed for the retrieving of the empirical relationships and probabilistic functions between a given SRI parameter (among three, one of these computed in two different ways) and the damage severity level based on (monitoring/survey) data collected for 706 masonry buildings on either shallow or piled foundations. The evaluation of the different SRI parameters represents a step forward with respect to previous studies that introduced the combined use of DInSAR and in-situ damage survey data to generate empirical fragility curves for (differential) settlement-affected buildings (Peduto et al., 2016a, 2017c, 2018b). Indeed, some considerations on the commonly used SRI parameters and the effects on the superstructure associated with their magnitude are suggested hereafter based on the empirical relationships and probabilistic functions obtained for such a rich dataset.

In order to identify the DInSAR-derived SRI parameter – among δρ, θ and Δ_1/L_1 (or, equally, Δ_2/L_2) – which, most properly, allows for (i) an analysis of the current damage

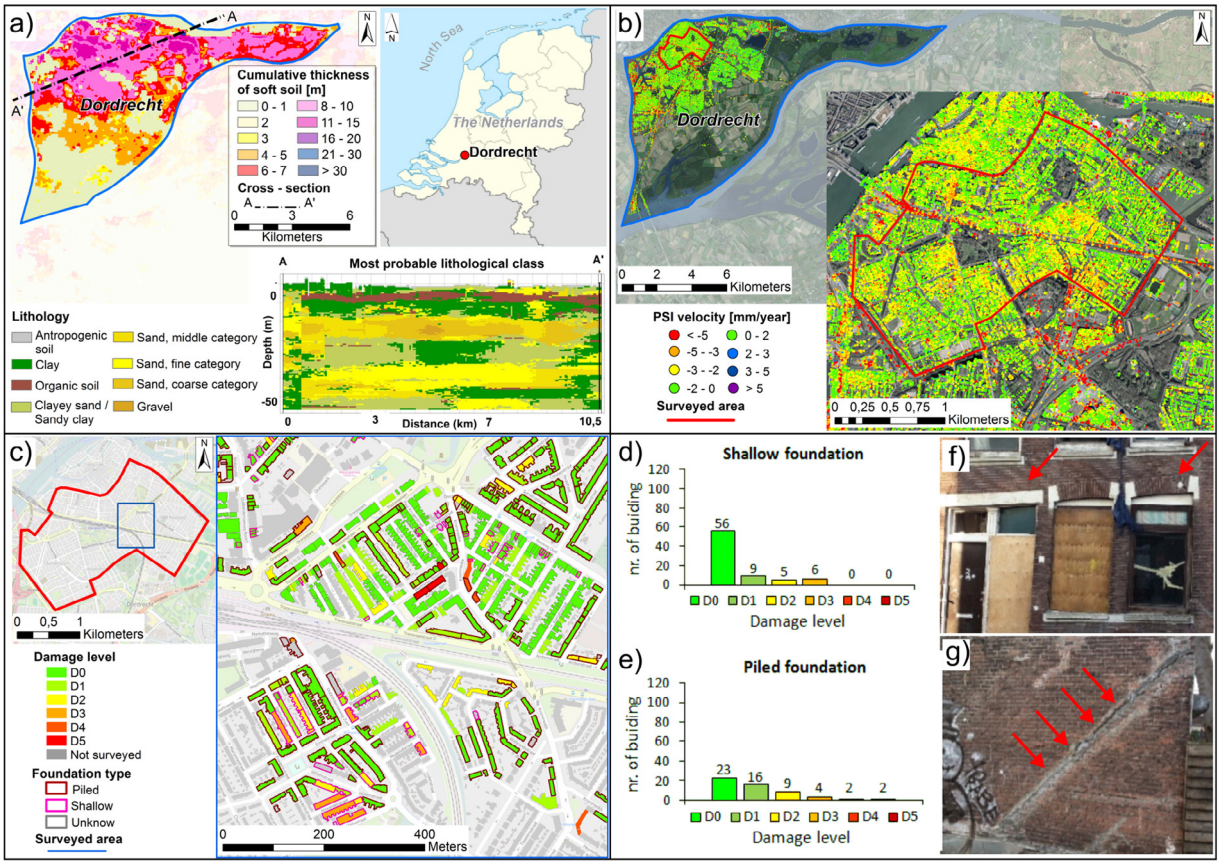

Fig. 8. Dordrecht case study: (a) cumulative thickness of soft soils (organic and clayey) and geological cross-section along the A–A′ profile sketch; (b) PSI data on the ascending orbit on top of the buildings provided by the TerraSAR-X radar sensor; (c) map of the surveyed masonry buildings distinguished according to the assigned damage severity level, foundation type and their distribution for (d) shallow and (e) piled foundations; (f) and (g) some photos of cracks and deformation revealed on building façades during the in-situ surveys.

Table 1
Number of surveyed buildings for each study area distinguished by the foundation type.

Surveyed buildings		
Case study	Foundation type	
	Shallow	Piled
Zaanstad	0	81
Rotterdam	0	183
Schiedam	104	206
Dordrecht	76	56
Total	**180**	**526**

severity level exhibited (on average) by the masonry buildings and (ii) a prediction of the damage severity level that might be experienced by a given (i.e., randomly selected) masonry building in the study areas, the values for μ and CV (from the empirical relationships) and β (from the fragility curves) for every SRI parameter are compared hereafter.

Focusing on the deflection ratios (Δ_1/L_1 and Δ_2/L_2), it can be observed that the empirical relationships (see Fig. 9e–h and Table 2) and the fragility curves (see Figs. 10e–h and 11e–h) are not markedly influenced by the use of Δ_1/L_1 or Δ_2/L_2. In particular, both series of arithmetic mean, standard deviation and CV (Table 2), as well as the values for the fragility parameters (Table 3), referring to different damage severity levels, exhibit slight differences based on whether either Δ_1/L_1 or Δ_2/L_2 is assumed as the SRI parameter. This would suggest that, based on the information on the DInSAR data and the damage severity level available in the present study, it could be sufficient to compute the deflection ratio according to the simplified approach (Δ_1/L_1) that does not require knowledge of all the points of inflection in the cumulative settlement trough along a section of a given building.

Fig. 9a–h highlight the idea that δρ seems to be the SRI parameter that works the best since its arithmetic mean values can be more easily associated with distinct damage severity levels when compared to the other SRI parameters. Moreover, for each damage severity level and both foundation typologies, the lowest values of CV (associated with the highest precision) are attained for the δρ parameter, whereas the highest ones (associated with the lowest precision) are recorded for the θ parameter. Overall, for a given SRI parameter, almost similar increasing trends of damage severity can be appreciated (on average) for both foundation systems (shallow and piled).

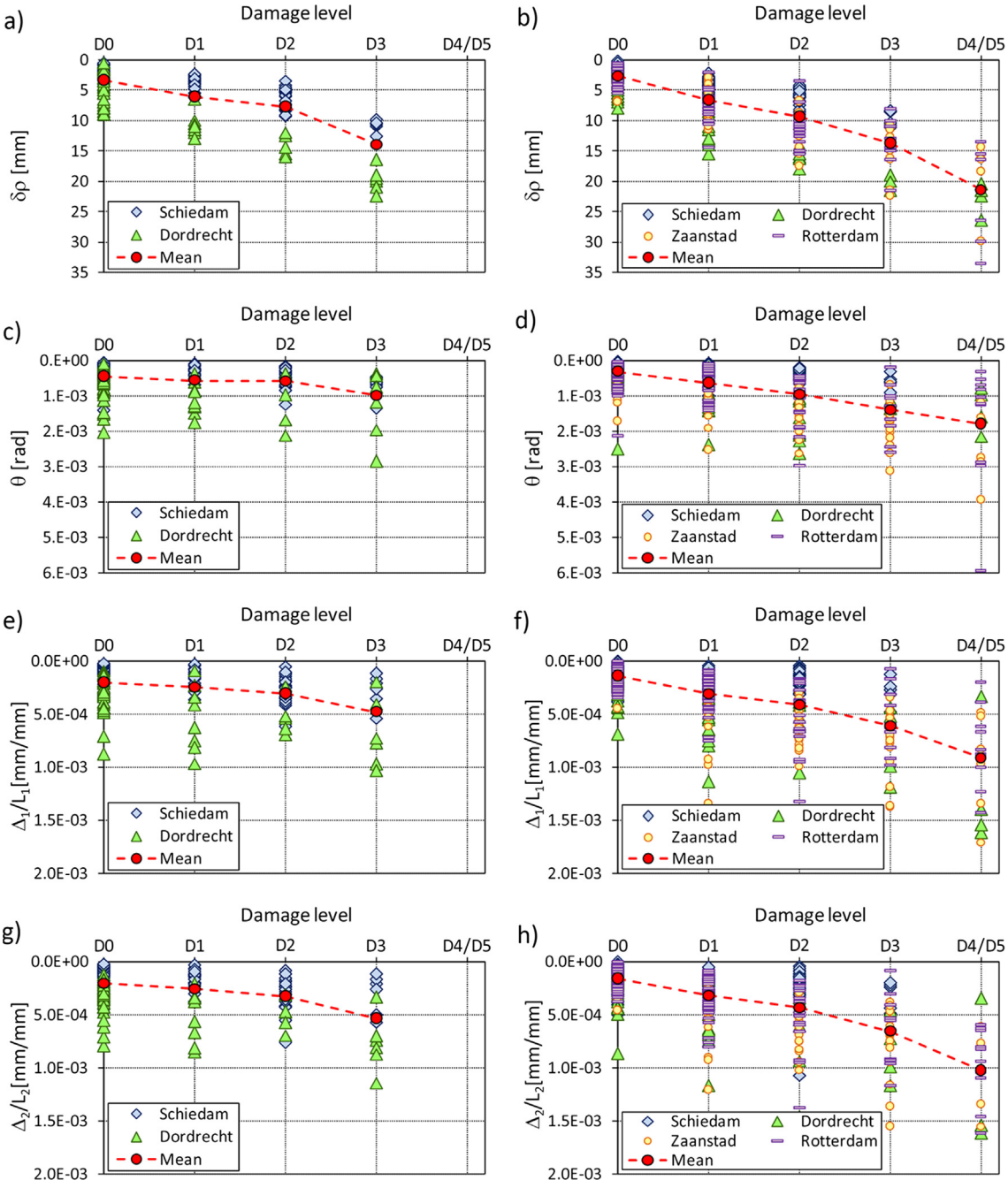

Fig. 9. Damage level vs. SRI parameters for (a), (c), (e) and (g) shallow and (b), (d), (f) and (h) piled foundations.

It can also be observed that, for any given SRI parameter, the β values (representing the dispersion of the results according to Fotopoulou and Pitilakis, 2013) are higher for shallow foundations than for piled ones. This reveals that the considered sample of buildings on shallow foundations is less statistically homogeneous than the one of buildings on piled foundations. Moreover, it is worth noting that, for θ, Δ_1/L_1 and Δ_2/L_2, the fragility curves (Figs. 10d, f and h and 11d, f and h) tend to be convex upward in shape (i.e., the existence of an inflection point cannot be clearly recognized), mainly develop horizontally, and the probability of reaching or exceeding a given damage severity level can attain the unit value (certainty) for unrealistic values of the considered SRI parameter with respect to the limiting values proposed in the literature (Grant et al., 1974; Polshin and Tokar, 1957; Skempton and MacDonald, 1956). This adversely affects the use of the obtained fragility curves for θ, Δ_1/L_1 and Δ_2/L_2 for forecasting purposes. On the contrary, the fragility curves generated using the δρ parameter for piled foundations (that exhibit all the analysed levels of damage severity) show that when δρ reaches a value equal to 100 mm, the probability of reaching or exceeding damage levels D1 to D4/D5 falls in the range of 90–100%. Somewhat surprisingly, values of δρ higher

Table 2
Arithmetic mean (μ), standard deviation (σ) and coefficient of variation (C_v) of the empirical relationships for each considered SRI parameter distinguished by the foundation type and damage level.

SRI parameter	Damage level	Foundation type					
		Shallow			Piled		
		μ	σ	CV	μ	σ	CV
δρ [mm]	D1	6.05	3.42	0.56	6.62	2.90	0.44
	D2	7.71	3.42	0.44	9.38	3.88	0.42
	D3	15.30	4.88	0.32	14.12	4.19	0.30
	D4/D5	–	–	–	25.68	11.93	0.46
θ [rad]	D1	2.16×10^{-4}	3.36×10^{-4}	1.55	2.19×10^{-4}	2.15×10^{-4}	0.98
	D2	1.89×10^{-4}	1.93×10^{-4}	1.02	2.92×10^{-4}	3.93×10^{-4}	1.35
	D3	3.34×10^{-4}	2.00×10^{-4}	0.60	5.21×10^{-4}	5.63×10^{-4}	1.08
	D4/D5	–	–	–	5.15×10^{-4}	5.03×10^{-4}	0.98
Δ_1/L_1 [mm/mm]	D1	2.50×10^{-4}	2.42×10^{-4}	0.97	3.08×10^{-4}	2.20×10^{-4}	0.71
	D2	3.05×10^{-4}	1.66×10^{-4}	0.54	4.20×10^{-4}	2.94×10^{-4}	0.70
	D3	4.80×10^{-4}	3.23×10^{-4}	0.67	6.43×10^{-4}	3.36×10^{-4}	0.52
	D4/D5	–	–		9.44×10^{-4}	4.06×10^{-4}	0.43
Δ_2/L_2 [mm/mm]	D1	2.58×10^{-4}	2.12×10^{-4}	0.82	3.22×10^{-4}	2.14×10^{-4}	0.67
	D2	3.27×10^{-4}	1.71×10^{-4}	0.52	5.98×10^{-4}	3.92×10^{-4}	0.65
	D3	5.37×10^{-4}	3.24×10^{-4}	0.60	6.92×10^{-4}	3.59×10^{-4}	0.52
	D4/D5	–	–	–	1.04×10^{-3}	4.06×10^{-4}	0.39

than approximately 30 mm have only been found for buildings with piled foundations, leading to a higher probability of reaching or exceeding damage severity level D4/D5 than those on shallow foundations. This may be caused by the loss of functionality of single piles due to wood decay processes in correspondence of which settlements concentrate. Apparently, shallow foundations exhibit settlements that are more uniformly distributed (i.e., effects that are less localized). The more localized settlements of the piled buildings are confirmed by the higher values for θ, Δ_1/L_1 and Δ_2/L_2, which can better explain the damage due to differential settlement.

Comparing the different municipalities, for buildings on shallow foundations (Fig. 9a, c, e and g), the SRI parameters attain their minimum values in Schiedam, whereas their maximum values are reached in Dordrecht probably due to the driving force of the groundwater lowering (see Section 5.4) which increases the effective stress pertaining to the subsoil. Buildings in Dordrecht seem to have suffered less damage than those in Schiedam for the same value of SRI parameters. Since the considered (subsample of) buildings have a homogeneous superstructure and foundation (i.e., shallow) typology, the above different behaviours could be related to the specific role played by other factors, such as slight differences in the underlying soil deposits and the age of the buildings in the two municipalities.

The curves in terms of the δρ obtained for the case study at hand were then compared with the ones proposed by Zhang and Ng (2005), who derived empirical fragility curves for a sample of 95 buildings (71 buildings with shallow foundations and 25 with piled foundations). Zhang and Ng (2005) assumed the maximum vertical settlement (ρ) as the SRI parameter. It was recorded by a sample of buildings collected in case histories available in the literature and included different structural typologies and varying subsoil conditions. As expected, the comparison (Fig. 12a and b) highlights that for buildings on both shallow and piled foundations, the empirical curves expressed as a function of δρ provide the probabilities of reaching or exceeding any given level of damage severity that is higher than either the limiting tolerable or the intolerable settlement (ρ), the latter affecting the functionality/safety of buildings according to Zhang and Ng (2005). This seems to confirm the different roles played by settlements and differential settlements on building damageability. Moreover, it should be noted that the sample of buildings considered by Zhang and Ng (2005) was more heterogeneous since it included masonry and (more recent) steel and reinforced concrete superstructures that, for a given value of (differential) settlement, can exhibit lower levels of damage severity. On the other hand, the DInSAR-derived settlement data, although accurate if compared with traditional settlement markers (see Fig. 1), only cover a period of about 5 years, whereas the damage to the houses may have cumulated over much longer periods, as most of these houses are between 35 and 100 years old. This may have led to an overestimation of the damage category related to the mea-

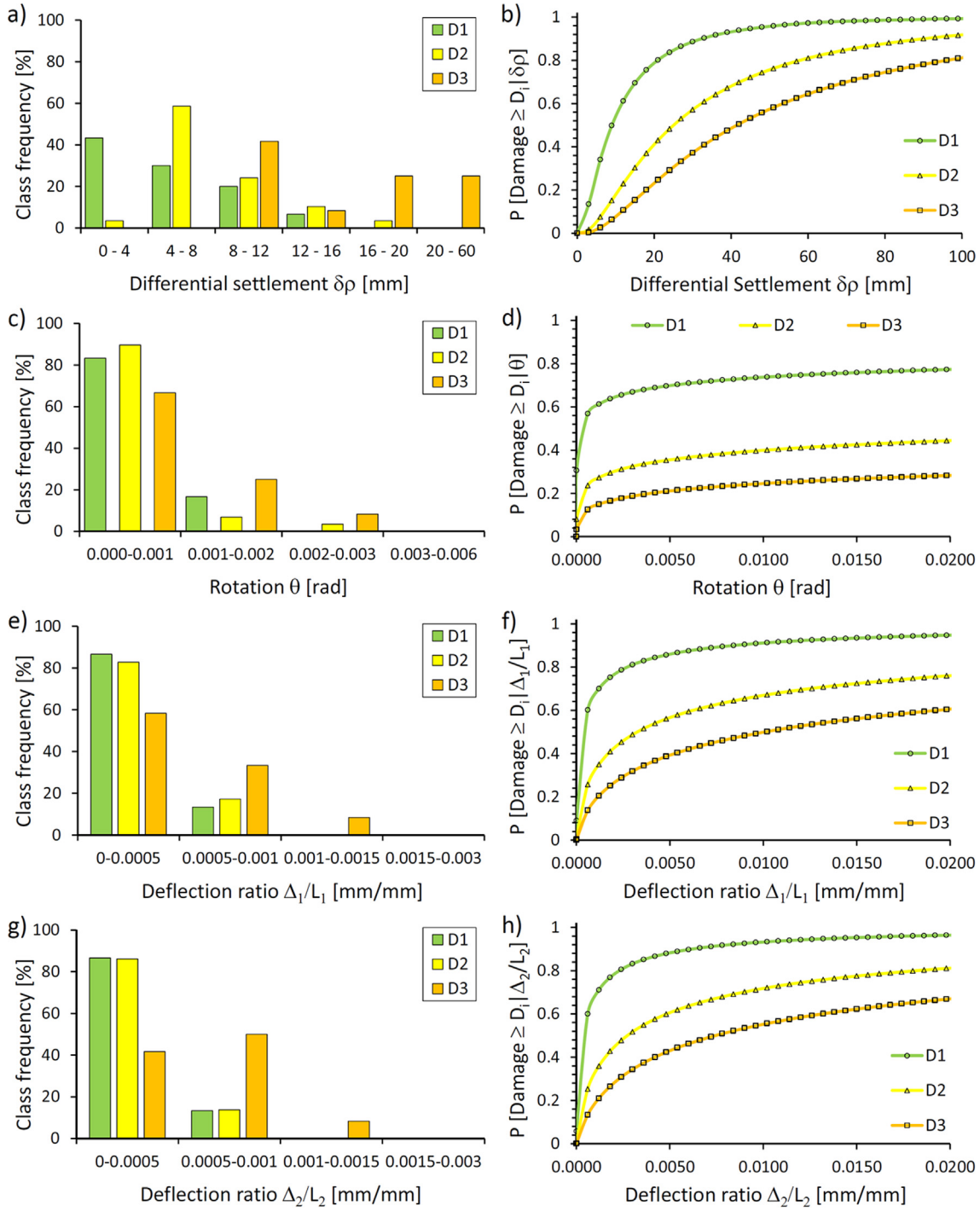

Fig. 10. Results of PSI-derived SRI parameters and damage survey relationship for single buildings with shallow foundations. Class frequency of damage severity level Di assigned to buildings for each considered SRI parameter: (a) differential settlement δρ, (c) rotation θ, (e) deflection ratio Δ_1/L_1, and (g) deflection ratio Δ_2/L_2; and fragility curves generated by using the log-normal distribution function for each considered SRI parameter: (b) differential settlement δρ, (d) rotation θ, (f) deflection ratio Δ_1/L_1, and (h) deflection ratio Δ_2/L_2.

sured parameter. From this point of view, more reliable results might be obtained by taking account of some relevant information – such as the age of construction, the damage severity progress over time for both the interior and exterior bearing walls (provided that knowledge on the date of the onset of damage is known) and possible measures taken to maintain/repair/replace the houses during the building life-cycle – not always available for a sample of 706 buildings. Indeed, the assigned damage severity refers to the damage visible only from the outside on building façades, and only one level was assumed for a single building. Accordingly, further deepening of the presented study is necessary in order to get to a refined analysis, including the assignment of a more accurate damage sever-

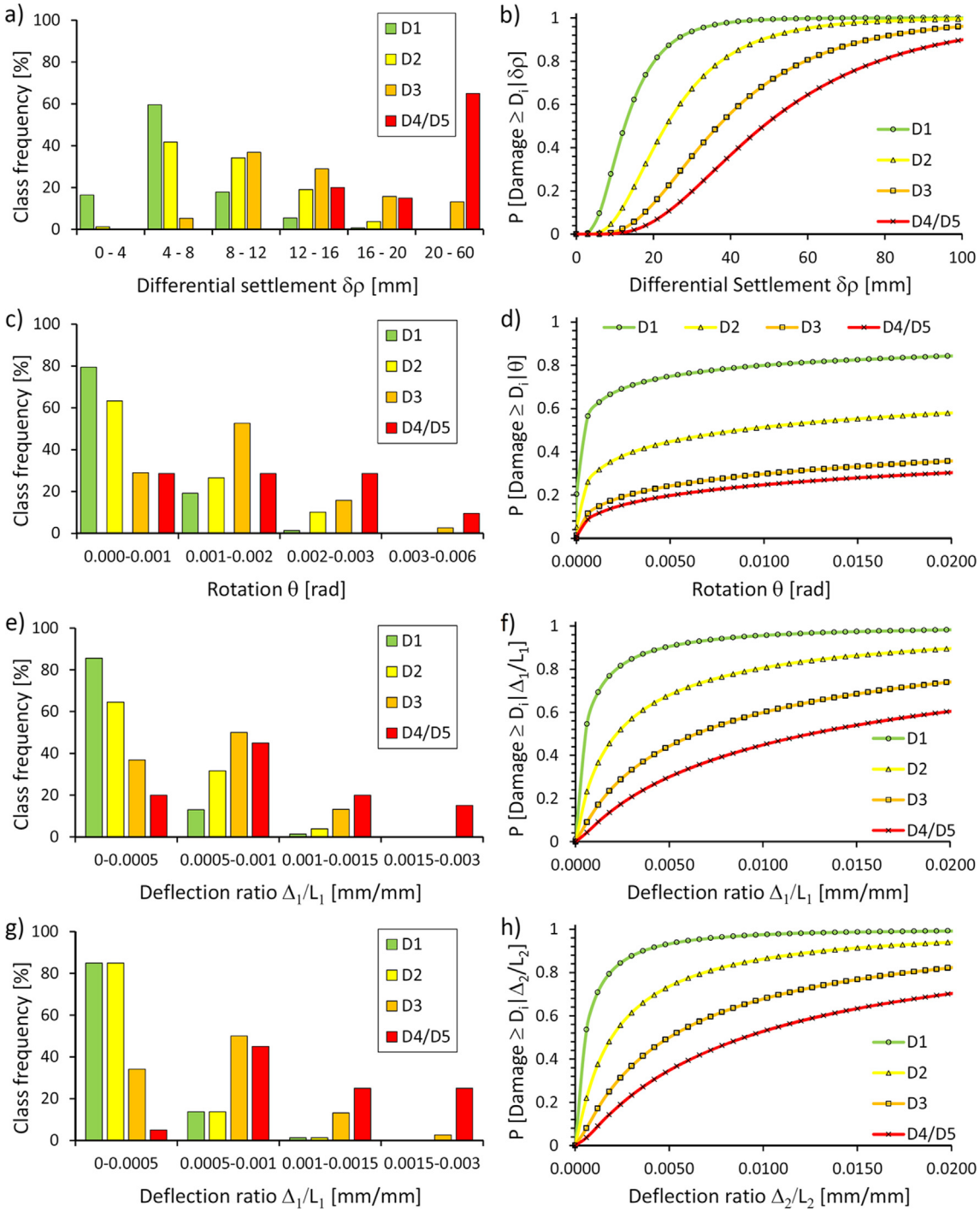

Fig. 11. Results of PSI-derived SRI parameters and damage survey relationship for single buildings with piled foundations. Class frequency of damage severity level Di assigned to buildings for each considered SRI parameter: (a) differential settlement δρ, (c) rotation θ, (e) deflection ratio Δ_1/L_1, and (g) deflection ratio Δ_2/L_2; and fragility curves generated by using the log-normal distribution function for each considered SRI parameter: (b) differential settlement δρ, (d) rotation θ, (f) deflection ratio Δ_1/L_1, and (h) deflection ratio Δ_2/L_2.

ity level distinguishing hogging or sagging modes of deformations. Moreover, other SRI parameters – such as horizontal strain (Boscardin and Cording, 1989) – should be considered, without neglecting the role of tilt (i.e., rigid body rotation) that a building might experience, in concurring to the attainment of serviceability/ultimate limit states. As for horizontal strain, wherever possible, the combination of DInSAR data on both ascending and descending orbits (Peduto et al., 2015, 2017c) would allow for the retrieval of the horizontal displacements that could also affect the development of damage in buildings (Boscardin and Cording, 1989; Burland et al., 2004).

Table 3
Median ($\overline{SRI}_i$) and standard deviation (β) of the lognormal distribution function for each considered SRI parameter distinguished by the foundation type and damage level.

SRI parameter	Damage level	Foundation type			
		Shallow		Piled	
		$\overline{SRI}_i$	β	$\overline{SRI}_i$	β
δρ [mm]	D1	9.04	0.99	12.57	0.57
	D2	25.06	0.99	23.26	0.57
	D3	41.53	0.99	36.81	0.57
	D4/D5	–	–	48.60	0.57
θ [rad]	D1	2.16×10^{-4}	6.04	3.10×10^{-4}	4.14
	D2	4.67×10^{-2}	6.04	8.69×10^{-3}	4.14
	D3	6.38×10^{-1}	6.04	9.08×10^{-2}	4.14
	D4/D5	–	–	1.69×10^{-1}	4.14
Δ_1/L_1 [mm/mm]	D1	3.16×10^{-4}	2.56	5.00×10^{-4}	1.76
	D2	3.26×10^{-3}	2.56	2.21×10^{-3}	1.76
	D3	1.01×10^{-2}	2.56	6.45×10^{-3}	1.76
	D4/D5	–	–	1.26×10^{-2}	1.76
Δ_2/L_2 [mm/mm]	D1	3.46×10^{-4}	2.25	5.32×10^{-4}	1.50
	D2	2.74×10^{-3}	2.25	1.95×10^{-3}	1.50
	D3	7.45×10^{-3}	2.25	5.01×10^{-3}	1.50
	D4/D5	–	–	9.00×10^{-3}	1.50

8. Conclusions

This paper presented a multi-parameter probabilistic approach to the analysis of damage in masonry buildings with different foundation types (either shallow or piled) in areas where the subsoil mainly consists of soft soils. For the purpose of the analysis, a damage survey dataset resulting from an extensive in-situ campaign of visual inspections was collected for more than 700 masonry buildings located in four municipalities in The Netherlands that have been dealing with settlement-induced damage for several decades. The damage survey results were combined with three different DInSAR-derived SRI parameters: differential settlement, rotation and deflection ratio (the latter was computed in two different ways) over the same sample of buildings in order to derive empirical relationships for the severity level of the recorded damage. This allowed for the enhancement of previous studies (Peduto et al., 2016a, 2017c), based on the analysis of a single SRI parameter (differential settlement), as well as for the identification of the SRI parameter (among the selected ones) that would be the most suitable for use in building settlement-induced damage analyses and predictions carried out following the proposed procedure. In particular, the observed results showed that, as expected, independent of the considered SRI parameter and building foundation typology, the severity level of the recorded damage increased as any SRI parameter increased. Moreover, the SRI parameter that was best related to the damage severity level assigned to the considered sample of buildings appeared to be the differential settlement. Indeed, it allowed for an easier and more precise estimation of the damage severity level pertaining (on average) to the investigated sample of masonry buildings and a more realistic predictability (based on the use of fragility curves) of the damage severity level that might be exhibited by a randomly selected masonry building in the study areas.

The main limitations to the practical applicability of the generated fragility curves would require (*i*) a better insight into the development over time of both damage levels and SRI parameters (i.e., the current damage level is compared with the values of the SRI parameters referring to a fixed period of time, although that damage may have developed in the past) and (*ii*) a more detailed damage survey (not limited to outer façades) in order to distinguish the behaviour of portions of buildings in sagging and hogging zones that could lead to an improved performance of the theoretically more correct SRI parameter like Δ_2/L_2.

Notwithstanding the above-mentioned limitations, the comparison conducted with the empirical fragility curves by Zhang and Ng (2005) pointed out the different roles played by settlements and differential settlements on the attainment of a given damage severity level as well as the importance of considering both the exact dating of the onset of damage, with respect to the period considered for the computation of cumulative settlements, and a homogeneous sample of buildings when performing probabilistic analyses.

Furthermore, the obtained results confirm the capability of DInSAR data to monitor and control the built-up environment with promising benefits in geotechnical engineering practice. Indeed, gathering the same amount of information through classic monitoring systems would have been unaffordable in terms of both time and money as confirmed by the limited number of buildings analysed in other scientific works that dealt with the same topic using the outcomes of conventional settlement monitoring data (see Section 2 for references therein).

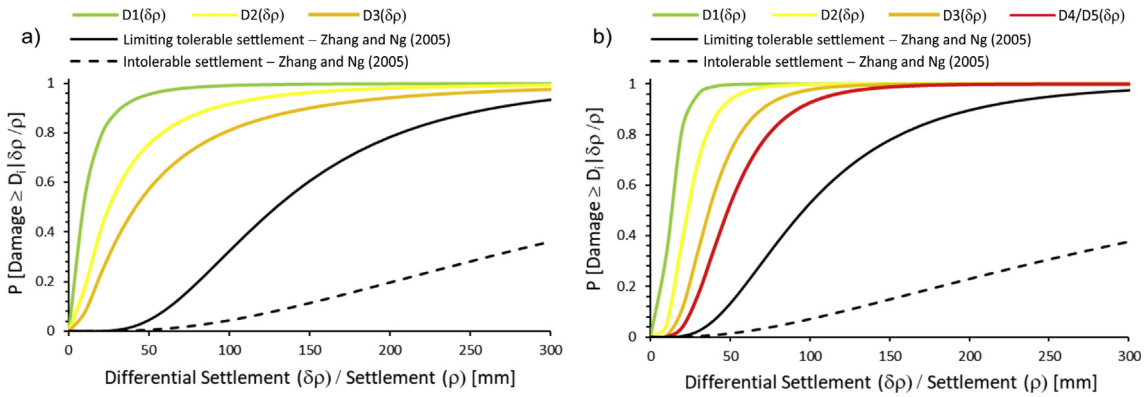

Fig. 12. Comparison of the proposed empirical fragility curve as a function of differential settlement (δρ) with the empirical curves as a function of settlement (ρ) provided by Zhang and Ng (2005) for (a) buildings with shallow foundations and (b) buildings with piled foundations.

The generated fragility curves, once further validated, could represent a useful tool for local authorities in charge of the management of subsidence-affected urban areas. Similarly, they could serve as a warning to homeowners of the potential development of damage, thereby helping to plan adequate measures to repair/replace foundations before the damage reached intolerable levels of severity.

Acknowledgements

This work was carried out also thanks to two ERASMUS+ for Traineeship Agreements between the University of Salerno (Italy) and Deltares (The Netherlands) and between the University of Salerno (Italy) and SkyGeo Netherlands B.V. The authors gratefully acknowledge SkyGeo Netherlands B.V for supplying the DInSAR data and the municipalities of Zaanstad, Rotterdam, Schiedam and Dordrecht for providing the traditional monitoring data and other background information. Many thanks are also offered to MSc students Sonia Colasante, Roberto D'Angelo and Francesco Pastore from the University of Salerno for their contribution to the building damage survey. Finally, the authors wish to thank the anonymous reviewers and the associate editor who provided useful suggestions for improving the paper to its final version.

References

AASHTO, 1997. Guide Specifications for Design of Pedestrian Bridges. American Association of State Highway and Transportation Officials, Washington, DC.

Bamler, R., Hartl, P., 1998. Synthetic aperture radar interferometry. Inverse Problems 14 (4), 1–54.

Bjerrum, L., 1963. Allowable settlement of structures. Proceedings of the 3rd European Conference on Soil Mechanics and Foundation Engineering, Wiesbaden, 2, Brighton, England, pp. 135–137.

Boscardin, M.D., Cording, E.G., 1989. Building response to excavation induced settlement. J. Geotech. Eng. 115, 1–21.

Bucx, T.H.M., van Ruiten, G., Erkens, G., de Lange, G., 2015. An integrated assessment framework for land subsidence in delta cities. In: Proc. IAHS, 372, Prevention and mitigation of natural and anthropogenic hazards due to land subsidence. Copernicus Publications on behalf of the International Association of Hydrological Sciences, pp. 485–491. https://doi.org/10.5194/piahs-372-485-2015.

Burland, J.B., Broms, B.B., de Mello, V.F.B., 1977. Behaviour of foundations and structures. In: SOA Report, Proc of the 9th Int Conf on Soil Mechanics and Foundation Engineering, Tokyo, vol. 2, pp. 495–546.

Burland, J.B., Mair, R.J., Standing, J.R., 2004. Ground performance and building response due to tunnelling, London. In: Proc of the Conference on Advances in Geotechnical Engineering. Thomas Telford Publisher, London, pp. vol. 1291–342.

Burland, J.B., 1995. Assessment of risk of damage to buildings due to tunnelling and excavation. Invited Special Lecture, Proceedings of the 1st International Conference on Earthquake Geotechnical Engineering, IS-Tokyo 95, pp. 1189–1201.

Burland, J.B., Wroth, C.P., 1974. Settlement of buildings and associated damage. SOA Review. Proc of the Conf on Settlement of Structures, Cambridge. Pentech Press, London, pp. 611–654.

Cascini, L., Ferlisi, S., Peduto, D., Fornaro, G., Manunta, M., 2007. Analysis of a subsidence phenomenon via DInSAR data and geotechnical criteria. Italian Geotech. J. XLI 4, 50–67.

Cascini, L., Peduto, D., Reale, D., Arena, L., Ferlisi, S., Verde, S., Fornaro, G., 2013. Detection and monitoring of facilities exposed to subsidence phenomena via past and current generation SAR sensors. J. Geophys. Eng. 10 (6). https://doi.org/10.1088/1742-2132/10/6/064001.

Castaldo, R., Tizzani, P., Lollino, P., Calo, F., Ardizzone, F., Lanari, R., Guzzetti, F., Manunta, M., 2015. Landslide Kinematical analysis through inverse numerical modelling and differential SAR interferometry. Pure Appl. Geophys. 172 (11), 3067–3080. https://doi.org/10.1007/s00024-014-1008-3.

CEN, 2004. Eurocode 7: Geotechnical design - Part 1: General rules. Final Draft, EN 1997-1:2004 (E), (F) and (G), November 2004. European Committee for Standardization, Brussels, p. 168.

Costantini, M., Falco, S., Malvarosa, F., Minati, F. 2008. A new method for identification and analysis of persistent scatterers in series of SAR images. In: IEEE International Geoscience & Remote Sensing Symposium, July 6–11, 2008, Boston, Massachusetts, USA. pp. 449–452.

Den Haan, E.J., Kruse, G.A.M., 2006. Characterisation and engineering properties of Dutch peats. In: Tan, T.S., Phoon, K.K., Hight, D.W., Leroueil, S. (Eds.), Characterization and Engineering Properties of Natural Soils 3. Taylor & Francis Group, London, pp. 2101–2133.

DINOloket, 2016. Data and information on the Dutch subsurface. Open data portal of the geological survey of the Netherlands. <https://www.dinoloket.nl/en> (accessed 03.04.2017).

Ferretti, A., Prati, C., Rocca, F., 2001. Permanent scatterers in SAR interferometry. IEEE Trans. Geosci. Remote Sens. 39 (1), 8–20.

Ferlisi, S., Nicodemo, G., Peduto, D., 2018. Empirical fragility curves for masonry buildings in slow-moving landslide-affected areas of southern Italy. In: Kallel, A., Ksibi, M., Ben Dhia, H., Khélifi, N. (Eds.) Recent Advances in Environmental Science from the Euro-Mediterranean and

Surrounding Regions. Proceedings of Euro-Mediterranean Conference for Environmental Integration (EMCEI-1) – Sousse (Tunisia), 22-25 November 2017. Advances in Science, Technology & Innovation (IEREK Interdisciplinary Series for Sustainable Development). Springer International Publishing AG, Cham, pp. 1825–1828.

Fornaro, G., Reale, D., Verde, S., 2013. Bridge thermal dilation monitoring with millimeter sensitivity via multidimensional SAR imaging. IEEE Geosci. Remote Sens. Letters 10, 677–768.

Fornaro, G., Reale, D., Verde, S., Peduto, D., Arena, L., Ferlisi, S., 2014. Potentialities of the use of spaceborne radar systems in the monitoring of structures and infrastructures. In: IEEE Workshop on Environmental Energy and Structural Monitoring Systems (EESMS), Naples, 17–18 September 2014, pp. 69–72 https://doi.org/10.1109/EESMS.2014 (6923267).

Fotopoulou, S.D., Pitilakis, K.D., 2013. Fragility curves for reinforced concrete buildings to seismically triggered slow-moving slides. Soil Dynamics and Earthquake En gineering 48, 143–161.

Franzius, J.N., Potts, D.M., Addenbrooke, T.I., Burland, J.B., 2004. The influence of building weight on tunneling-induced ground and building deformation. Soils Foundat. 44 (1), 25–38.

Gehl, P., Douglas, J., Seyedi, D., 2015. Influence of the number of dynamic analyses on the accuracy of structural response estimates. Earthquake Spectra, Earthquake Eng. Res. Inst. 31 (1), 97–113.

Grant, R., Christian, J.T., Vanmarcke, E.H., 1974. Differential settlement of buildings. J. Geotech. Eng., ASCE 100 (9), 973–991.

Hanssen, F.R., 2003. Subsidence monitoring using contiguous and PS-INSAR: quality assessment based on precision and reliability. Proc. 11th FIG Symposium on Deformation Measurements, Santorini, Greece, pp. 1–8.

Hartemink, A.E., Sonneveld, M.P.W., 2013. Soil maps of The Netherlands. Geoderma, 1–9, 204–205.

Herrera, G., Fernandez-Merodo, J., Tomas, R., Cooksley, G., Mulas, J., 2009. Advanced interpretation of subsidence in Murcia (SE Spain) using A-DInSAR data-modelling and validation. Nat. Hazard. Earth Syst. Sci. 9, 647–661.

Holzer, T.L., 2009. Living with Unstable Ground. Environmental Awareness Series American Geosciences Institute Publication, pp. 68 (ISBN: 0-922152-82-9978-0-922152-82-7).

Klaassen, R.K.W.M., Creemers, J.G.M., 2012. Wooden foundation piles and its underestimated relevance for cultural heritage. J. Cultural Heritage 13, 123–128.

Mavrouli, O., Fotopoulou, S., Pitilakis, K., Zuccaro, G., Corominas, J., Santo, A., Cacace, F., De Gregorio, D., Di Crescenzo, G., Foerster, E., Ulrich, T., 2014. Vulnerability assessment for reinforced concrete buildings exposed to landslides. Bull. Eng. Geol. Environ. 73, 265–289.

Modoni, G., Darini, G., Spacagna, R.L., Saroli, M., Russo, G., Croce, P., 2013. Spatial analysis of land subsidence induced by groundwater withdrawal. Eng. Geol. 167, 59–71. https://doi.org/10.1016/j.enggeo.2013.10.014.

Nicodemo, G., Peduto, D., Ferlisi, S., Maccabiani, J., 2016. Investigating building settlements via very high resolution SAR sensors. In: Bakker, Frangopol, van Breugel (Eds.), Life-Cycle of Engineering Systems: Emphasis on Sustainable Civil Infrastructure. Taylor & Francis Group, London, pp. 2256–2263.

Papadaki, E., 2013. Modeling of Peat Compresses under Sand Bodies: Experimental and Numerical Approach Master thesis. Technical University Delft, The Netherlands, p. 216.

Peduto, D., Cascini, L., Arena, L., Ferlisi, S., Fornaro, G., Reale, D., 2015. A general framework and related procedures for multiscale analyses of DInSAR data in subsiding urban areas. ISPRS J. Photogramm. Remote Sens. 105, 186–210. https://doi.org/10.1016/j.isprsjprs.2015.04.001.

Peduto, D., Elia, F., Montuori, R., 2018a. Probabilistic analysis of settlement-induced damage to bridges in the city of Amsterdam (The Netherlands). Transp. Geotechn. 14, 169–182. https://doi.org/10.1016/j.trgeo.2018.01.002.

Peduto, D., Ferlisi, S., Nicodemo, G., Reale, D., Pisciotta, G., Gullà, G., 2017a. Empirical fragility and vulnerability curves for buildings exposed to slow-moving landslides at medium and large scales. Landslides 14 (6), 1993–2007. https://doi.org/10.1007/s10346-017-0826-7.

Peduto, D., Huber, M., Speranza, G., van Ruijven, J., Cascini, L., 2017b. DInSAR data assimilation for settlement prediction: case study of a railway embankment in The Netherlands. Canadian Geotech. J. 54 (4), 502–517. https://doi.org/10.1139/cgj-2016-0425.

Peduto, D., Nicodemo, G., Caraffa, M., Gullà, G., 2018b. Quantitative analysis of consequences to masonry buildings interacting with slow-moving landslide mechanisms: a case study. Landslides 15 (10), 2017–2030. https://doi.org/10.1007/s10346-018-1014-0.

Peduto, D., Nicodemo, G., Maccabiani, J., Ferlisi, S., 2017c. Multi-scale analysis of settlement induced building damage using damage surveys and DInSAR data: a case study in The Netherlands. Eng. Geol. 218, 117–133. https://doi.org/10.1016/j.enggeo.2016.12.018.

Peduto, D., Nicodemo, G., Maccabiani, J., Ferlisi, S., D'Angelo, R., Marchese, A., 2016a. Investigating the behaviour of buildings with different foundation types on soft soils: two case studies in The Netherlands. VI Italian Conference of Researchers in Geotechnical Engineering, CNRIG2016 -Geotechnical Engineering in Multidisciplinary Research: from Microscale to Regional Scale, 22–23 September 2016, Bologna (Italy). Procedia Eng. 158, 529–534. https://doi.org/10.1016/j.proeng.2016.08.484.

Peduto, D., Pisciotta, G., Nicodemo, G., Arena, L., Ferlisi, S., Gullà, G., Borrelli, L., Fornaro, G., Reale, D., 2016b. A procedure for the analysis of building vulnerability to slow-moving landslides. In: Daponte, P., Simonelli, A.L., (Eds.), Proc of the 1st IMEKO TC4 Int Workshop on Metrology for Geotechnics – Benevento, Italy, March 17–18, 2016, pp. 248–254.

Polshin, D.E., Tokar, R.A., 1957. Maximum Allowable Non-uniform Settlement of Structures. Proc. 4th Int. Conference Soil Mechanics and Foundation Engineering. Butterworths Scientific Publications, London, pp. 402–405.

Reale, D., Fornaro, G., Pauciullo, A., Zhu, X., Bamler, R., 2011. Tomographic imaging and monitoring of buildings with very high resolution SAR data. IEEE Geosci. Remote Sens. Lett. 8, 661–665.

Saeidi, A., Deck, O., Verdel, T., 2012. Development of building vulnerability functions in subsidence regions from analytical methods. Géotechnique 62 (2), 107–120. https://doi.org/10.1680/geot.9.P.028.

Shinozuka, M., Feng, M.Q., Kim, H.K., Uzawa, T., Ueda, T., 2003. Statistical Analysis of Fragility Curves. Technical report MCEER-03-0002. State University of New York, Buffalo.

Shinozuka, M., Feng, M.Q., Lee, J., Naganuma, T., 2000. Statistical analysis of fragility curves. J. Eng. Mech. 126 (12), 1224–1231.

Skempton, A.W., MacDonald, D.H., 1956. Allowable settlement of buildings. In: Proc. of the ICE (Institute of Civil Engineers), Pt. III, vol. 5, pp. 727–768.

Son, M., Cording, E.J., 2007. Evaluation of building stiffness for building response analysis to excavation-induced ground movements. J. Geotech. Geoenviron. Eng. 133 (8), 995–1002.

Stafleu, J., Maljers, D., Gunnink, J.L., Menkovic, A., Busschers, F.S., 2011. 3D modeling of the shallow subsurface of Zeeland, the Netherlands. Netherlands J. Geosci.-Geol. En Mijnbouw 90 (4), 293–310.

USGS, 2016. <http://dds.cr.usgs.gov/srtm/> (accessed 03.04.2017).

van der Meulen, M.J., Doornenbal, J.C., Gunnink, J.L., Stafleu, J., Schokker, J., Varnes, R.W., van Geer, F.C., van Gessel, S.F., van Heteren, S., van Leeuwen, R.J.W., Bakker, M.A.J., Bogaard, P.J.F., Busschers, F.S., Griffioen, J., Gruijters, S.H.L.L., Kiden, P., Schroot, B.M., Simmelink, H.J., van Berkel, W.O., van der Krogt, R.A.A., Westerhoff, W.E., van Daalen, T.M., 2013. 3D geology in a 2D country: perspectives for geological surveying in the Netherlands. Netherlands J. Geosci.-Geol. En Mijnbouw 92 (4), 217–241.

Zhang, L.M., Ng, A.M.Y., 2005. Probabilistic limiting tolerable displacements for serviceability limit state design of foundations. Geotéchnique 55 (2), 151–161.

Zhu, X., Bamler, R., 2010. Very high resolution spaceborne SAR tomography in urban environment. IEEE Trans. Geosci. Remote Sens. 48, 4296–4308.